

Vidarc: Embodied Video Diffusion Model for Closed-loop Control

Yao Feng^{1*}, Chendong Xiang^{1*}, Xinyi Mao¹, Hengkai Tan¹, Zuyue Zhang²,
 Shuhe Huang¹, Kaiwen Zheng¹, Haitian Liu¹, Hang Su^{1†}, Jun Zhu^{1†}

¹Dept. of Comp. Sci. and Tech., Institute for AI, BNRist Center, THBI Lab,
 Tsinghua-Bosch Joint ML Center, Tsinghua University

²School of Architecture, Tsinghua University

{y-feng23, xcd24}@mails.tsinghua.edu.cn, dcszj@tsinghua.edu.cn

Abstract

Robotic arm manipulation in data-scarce settings is a highly challenging task due to the complex embodiment dynamics and diverse contexts. Recent video-based approaches have shown great promise in capturing and transferring the temporal and physical interactions by pre-training on Internet-scale video data. However, such methods are often not optimized for the embodiment-specific closed-loop control, typically suffering from high latency and insufficient grounding. In this paper, we present Vidarc (Video Diffusion for Action Reasoning and Closed-loop Control), a novel autoregressive embodied video diffusion approach augmented by a masked inverse dynamics model. By grounding video predictions with action-relevant masks and incorporating real-time feedback through cached autoregressive generation, Vidarc achieves fast, accurate closed-loop control. Pre-trained on one million cross-embodiment episodes, Vidarc surpasses state-of-the-art baselines, achieving at least a 15% higher success rate in real-world deployment and a 91% reduction in latency. We also highlight its robust generalization and error correction capabilities across previously unseen robotic platforms.

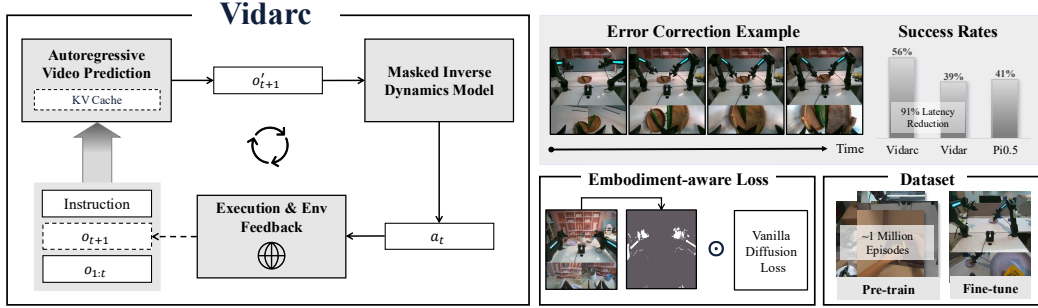


Figure 1: Left: Vidarc consists of an embodied autoregressive video diffusion model and a masked inverse dynamics model. To enable closed-loop control, the inference pipeline re-prefills environment feedback into the autoregressive video generation. Right: After being pre-trained on approximately one million bimanual demonstration episodes, Vidarc is fine-tuned on an unseen platform using calibration with embodiment-specific masks; it achieves state-of-the-art performance and exhibits robust error correction capabilities.

*Equal contribution; [†]The corresponding author.

1 Introduction

Robotic arm manipulation is a fundamental yet highly complex task, requiring precise coordination across multiple degrees of freedom to execute intricate movements in dynamic environments. In many real-world applications, such as autonomous assembly lines, medical surgery, or hazardous material handling, collecting large, high-quality datasets is prohibitively expensive or impractical, especially when adapting robotic control to new platforms, tasks, or environments. As a result, achieving robust and generalizable manipulation skills from limited data is a crucial goal, enabling widespread and scalable deployment of robotic systems [1, 2].

Inspired by the success of large language models, one effective approach in data-scarce settings is to leverage a pre-trained foundation model plus a fine-tuning step for knowledge transfer. Representative progress includes meta-learning [3], vision-language-action models which typically add action heads to pre-trained vision-language models [4, 5, 6, 7], as well as video generation models with lightweight embodied-specific controllers or inverse dynamics models [8, 9]. Among these approaches, video generation models have shown great promise by fully exploring the Internet-scale video data, while the others often have to collect a large set of human demonstration data. Videos, unlike static images or discrete trajectory representations, capture the full temporal dynamics and interaction cues essential for manipulation tasks. Trained on massive video datasets [10, 11, 12], video generation models create transferable priors that enforce physical consistency, support counterfactual reasoning, and can be efficiently fine-tuned with very few demonstrations [8].

This progress notwithstanding, little progress has been made so far on the real-time, embodiment-specific requirements of robotic control. Closed-loop control is highly desired and especially important in robotics [13, 14, 15, 16] because it enables the system to constantly refine its actions based on new sensory feedback, greatly increasing robustness to unexpected environmental changes, errors, or perturbations. Achieving this with video foundation models poses unique challenges: it requires low-latency generation, seamless integration of real-time feedback, and quick adaptation to embodiment-specific cues within the video stream. Previous approaches often focused on open-loop prediction or required slow, sequential inference, making them impractical for real-world, interactive robot tasks [17]. Moreover, pure video generative models typically lack grounding in embodiment-relevant dynamics and visual features; subtle visual or physical deviations—such as minor changes in the robot arm’s appearance or pose—can cause dramatic task failures if not properly accounted for [18].

To address these limitations, we propose **Vidarc** (Video Diffusion for Action Reasoning and Closed-loop Control), which consists of an autoregressive embodied video diffusion model and a masked inverse dynamics model. By incorporating environmental feedback in the autoregressive generation process with key-value (KV) caching, Vidarc enables robust closed-loop control with low latency during inference. To further ground the video diffusion model in the specific dynamics of a robot, we use learned action-relevant masks from the masked inverse dynamics model to construct an embodiment-aware diffusion loss, ensuring the generated videos are actionable. We illustrate our method in Figure 1.

With large-scale cross-embodiment pre-training on approximately one million episodes, Vidarc adapts to an unseen real-world platform with superior success rates than strong baselines: 17% higher than Vidar [8] and 15% higher than Pi0.5 [5]. Furthermore, Vidarc only incurs 8.8% of Vidar’s latency, with remarkable generalization and error correction capabilities.

2 Preliminary

We start by briefly summarizing the preliminary knowledge.

2.1 Diffusion Model

Diffusion model designs a noise injection and denoise process to generate high-quality images or videos. Modern video diffusion models [10, 19] adopt the flow matching framework [20, 21], which enables stable training with the ordinary differential equation (ODE) formulation. Given a video x_1 , a random Gaussian noise x_0 with the same size, and a timestep $t \in [0, 1]$, we define the noised video x_t as $tx_1 + (1 - t)x_0$. Let \mathcal{V} be the video space, and \mathcal{C} be the condition space. The diffusion model

learns a flow function $v_\theta : \mathcal{V} \times \mathbb{R} \times \mathcal{C} \rightarrow \mathcal{V}$, which parameterizes the vector field that transforms x_1 to x_0 given the intermediate x_t and t and condition c . The training objective is:

$$\mathcal{L}_{\text{diffusion}} = \mathbb{E}_{x_0, x_1, t, c} [\|v_\theta(x_t, t, c) - (x_0 - x_1)\|_2^2]. \quad (1)$$

During inference, we can sample from the learned distribution by solving the following ODE from $t = 0$ to $t = 1$ by using efficient training-free solvers [22, 23]:

$$\frac{dx_t}{dt} = v_\theta(x_t, t, c), \quad t \in [0, 1]. \quad (2)$$

Thanks to their strong ability to model complex spatial-temporal dynamics, video diffusion models can serve not only as generative models but also as world models that simulate the evolution of visual environments. Recent works have demonstrated their potential for interactive prediction and control, such as physical simulation [24, 25] and robotic manipulation planning [8, 17]. As both model capacity and training data scale up, video diffusion models exhibit emerging properties including zero-shot generalization and chain-of-frames reasoning [26], suggesting promising applicability to complex real-world manipulation and reasoning tasks.

2.2 Video-based Action Prediction

In video-based approaches, video diffusion models form the backbone, with actions derived either from an action head, which takes latent vectors as input [27], or from an Inverse Dynamics Model (IDM) [28], typically predicting actions \hat{a} from images x . However, only the robotic arm’s key regions are necessary for action prediction in these images, while other areas may introduce noise that interferes with model performance. To address this, Vidar [8] introduces a masked inverse dynamics model (MIDM) approach, which employs a mask predictor U to predict a mask $m \in [0, 1]$ that highlights action-relevant pixels, together with an action regressor R for action regression:

$$m = U(x), \quad \hat{a} = R(\text{Round}(m) \odot x), \quad (3)$$

where ‘‘Round’’ is the rounding function. This masking mechanism preserves critical motion-related regions and suppresses irrelevant visual information, thereby enhancing the accuracy and robustness of action prediction in the IDM. Since the mask is closely tied to the robot’s dynamics, it offers a more effective prior than general segmentation models. In the training process, Vidar regularizes the area of m with a weight of λ :

$$\mathcal{L}_{\text{action}} = \mathbb{E}_{x, a} [l(\hat{a} - a) + \lambda \|m\|_1], \quad (4)$$

where $l(\cdot)$ is the Huber loss. Generally, the IDM handles robot-specific action spaces and control signals, while video diffusion models focus on unified video generation tasks, where abundant prior knowledge is transferred from pre-training.

3 Method

Although recent video world models have shown remarkable generalization across visual domains, their architectures are inherently not optimized for embodied control. Most of these methods rely on bidirectional diffusion mechanisms, which lack causality and suffer from high per-frame latency [29], global dependencies, and cumulative prediction errors in long-horizon sequences [30, 31, 32, 33]. Moreover, the conventional diffusion training paradigm treats all visual features equally, ignoring the asymmetric, motion-dependent structure of physical interaction—a property essential for stable and efficient action generation.

In contrast, a robot-native policy must process environmental feedback in a causal and low-latency manner, enabling rapid perception-action cycles and continuous adaptation to dynamic surroundings. It should exhibit strong inductive biases for motion and kinematics, ensuring physically consistent trajectories, while maintaining computational efficiency to support real-time inference and robust generalization across diverse scenarios.

To meet these requirements, Vidarc builds upon causal autoregressive frame prediction with re-prefilling to enable closed-loop interaction with minimal latency. By re-prefilling observations from the environment, we can bridge the inherent training-inference gap in autoregressive models, preventing error accumulation and accounting for environmental changes. Further enhanced with an embodiment-aware loss, our model explicitly emphasizes motion dynamics during training, leading to more stable, efficient, and adaptive embodied behavior.

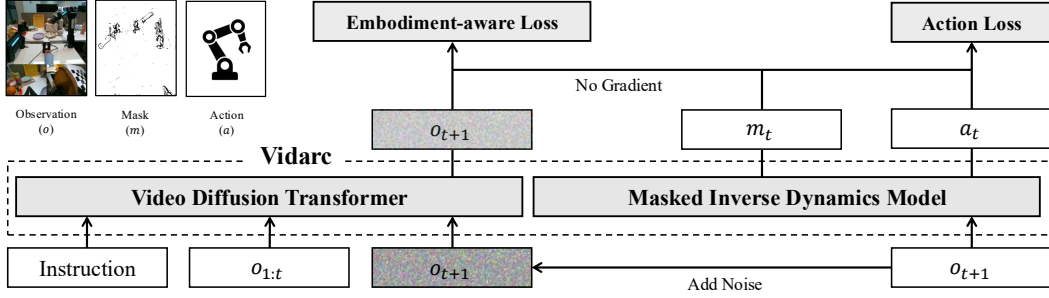


Figure 2: Vidarc comprises a video diffusion transformer and a masked inverse dynamics model. The video diffusion transformer is trained via teacher-forcing to predict the next observation based on previous observations and language instructions, while the masked inverse dynamics model is trained to infer actions from observations using a learnable masking mechanism that focuses attention on action-relevant regions. The learned mask is also used to reweight the diffusion loss, enhancing the video model’s focus on regions important for action prediction.

3.1 Model Design

Figure 2 presents an overview of our method. Specifically, let \mathcal{L} be the language instruction space, \mathcal{O} be the chunked visual observation space (a sequence of images with a chunk size ≥ 1), and \mathcal{A} be the chunked action space (a sequence of actions with a chunk size ≥ 1). We target to learn a conditional robot manipulation policy $\pi : \mathcal{L} \times \mathcal{O} \rightarrow \mathbb{P}(\mathcal{A})$. Similar to previous video-based methods [17], we decompose it into two models: $\pi = G \circ I$, where $G : \mathcal{L} \times \mathcal{O} \rightarrow \mathbb{P}(\mathcal{O})$ is a video generation model and $I : \mathcal{O} \rightarrow \mathcal{A}$ is an inverse dynamics model. The inverse dynamics model is typically modeled as a mapping from image to action; with a slight abuse of notation, we also use the term “inverse dynamics model” to refer to the batch application of image chunks as input.

To adopt closed-loop control, we propose to take the feedback from the environment into the pipeline. Assuming the transition function is $\mathcal{T} : \mathcal{O} \times \mathcal{A} \rightarrow \mathcal{O}$ and the observation aggregation function is $\mathcal{C} : \bigsqcup_{n=1}^{\infty} \mathcal{O}^n \rightarrow \mathcal{O}$, we can unroll the policy for timestep t as follows:

$$\begin{cases} \hat{o}_{t+1} \sim G(l, \mathcal{C}(o_1, \dots, o_t)) & \# \text{Autoregressive Generation} \\ a_t = I(\hat{o}_{t+1}) & \# \text{Inverse Dynamics Decoding} \\ o_{t+1} = \mathcal{T}(o_t, a_t) & \# \text{Execution and Collection}, \end{cases} \quad (5)$$

where o_1 is the initial observation. Specifically, we first generate the next observation \hat{o}_t based on the instruction l and the aggregation of previous observations. Then we decode the action a_t from the generated observation \hat{o}_t . Finally, we execute the action a_t in the environment and collect the new observation o_{t+1} .

3.2 Training

We outline the training of the video diffusion transformer.

Causal Training To enable causal generation, we utilize the CausVid [33] method, transfer the text-image to video model to a frame-by-frame generation model. During the generation of each frame, all previous frames of this frame (x_{prev}) are noise-free (i.e., already denoised) and can be attended to in the attention operation. The causal training objective is:

$$\mathcal{L}_{\text{causal}} = \mathbb{E}_{x_0, x_1, t, c} [\|v_{\theta}(x_t, t, c, x_{prev}) - (x_0 - x_1)\|_2^2]. \quad (6)$$

Embodiment-aware Loss As shown in Figure 3, Video diffusion models suffer from inaccurate modeling of robot-relevant features, which are crucial for precise control. To address this issue, we propose an embodiment-aware loss that enhances the video diffusion model’s focus on action-relevant regions. In this way, the model is adapted to the specific embodiment, enabling the generation of more actionable videos.

Algorithm 1 Inference Algorithm of Vidarc

```
1: Input: Environment  $E$ , Instruction  $l$ , Autoregressive model  $G$ , Inverse Dynamics Model  $I$ 
2: Hyperparameters: Chunk size  $n\_c$ , Maximum KV length  $n\_k$ 
3: while task not complete and not timeout do
4:    $o_1 \leftarrow E.get\_obs()$ 
5:    $C = \{c_1\} \leftarrow G.prefill(o_1)$  # Initialize the KV cache with the first observation
6:   for  $i = 1$  to  $n\_k$  step  $n\_c$  do
7:      $gen\_obs \leftarrow []$ 
8:     for  $j = i + 1$  to  $i + n\_c$  do
9:        $o'_j, c'_j \leftarrow G.generate(l, C)$  # Generate with KV cache
10:       $gen\_obs.append(o'_j); C.append(c'_j)$ 
11:    end for
12:     $a \leftarrow I(gen\_obs)$ 
13:     $E.execute(a)$ 
14:     $C.pop\_back(n\_c)$  # Remove the last chunk of the KV cache
15:     $gt\_obs = \{o_{i+1}, \dots o_{i+n\_c}\} \leftarrow E.get\_obs()$  # Get ground truth observations
16:     $C \leftarrow G.chunk\_prefill(C, gt\_obs)$  # Re-prefill with ground truth observations
17:  end for
18:   $C.clean()$  # Reset the KV cache
19: end while
```

Inspired by the masked inverse dynamic model, the mask m highlights regions relevant to the robot's actions, such as the robot arm. We use the learned mask to reweight the diffusion loss, encouraging the video model to pay more attention to these critical areas. The final training objective is

$$\mathcal{L}_{\text{embodiment-aware}} = \mathbb{E}_{x_0, x_1, t, c} [\|(1 + \eta \cdot U(x_1)) \odot (v_\theta(x_t, t, c, x_{\text{prev}}) - (x_0 - x_1))\|_2^2], \quad (7)$$

where η is a hyperparameter controlling the strength of the reweighting.

In this way, the video diffusion model is guided to focus on action-relevant regions, also matching the masked prediction of the inverse dynamics model (details in Section 2.2), leading to improved performance in precise control tasks.



Figure 3: Video predictions often get artifacts around the robot arm, which affects the task success.

3.3 Inference

The general inference pipeline is described by equation 5, with our detailed implementation provided in Algorithm 1. In particular, we generate the next observation based on previous real-world observations, rather than generated ones, enabling closed-loop control. This paradigm aligns with teacher forcing training, incorporating inference to prevent error accumulation.

To accelerate the generation process, we employ KV caching and cache instruction embeddings, thereby avoiding redundant recomputation across decoding steps. To further reduce inference latency, we introduce a re-prefill mechanism that optimizes the prefill phase: rather than recomputing KV caches for the entire sequence of prior observations, we only pop the latest generated KV cache, and then perform chunk prefill with the latest observations. In this way, the step sequence length for prefilling is significantly reduced, saving the computation cost and reducing the latency.

4 Experiments

We now present experimental results with the goal to verify the following claims:

- C1:** Vidarc achieves superior success rates on both simulated and real domains;
- C2:** Vidarc generalizes effectively to unseen tasks and environments;
- C3:** Vidarc achieves low-latency closed-loop control with error correction abilities;
- C4:** The embodiment-aware diffusion loss enhances Vidarc’s ability.

4.1 Experimental Setup

Hardware. We choose the widely used Aloha robot [34, 6] as our target platform, with three cameras providing multi-view observations. The action for the robot is the target absolute joint position, and does not depend on history. Detailed hardware configurations are in Appendix D.

Datasets. For pretraining, we use a curated dataset of one million video clips, sampled from four diverse sources: Egodex [35], Agibot [36], RDT [6], and RoboMind [37]. This large-scale, multi-domain pretraining enables the model to learn rich visual and temporal representations of robotic and human interactions. For finetuning data, finetuning is performed in two domain-specific datasets , including simulation and real-world:

- RoboTwin: We collect 20 episodes for each task on the agilex Aloha platform, resulting in a total of 1,000 episodes.
- Vidarc: We collected 2,307 episodes of high-quality, real-world robot operation data on our Aloha robot platform.

More details of the datasets are shown in Appendix A.

Baselines. To ensure fair and meaningful comparisons, we implement two competitive baselines:

- Vidar [8]: We replicate the Vidar approach using Wan2.2 [10] backbone. This baseline undergoes 10k steps of continued pretraining on our pretraining dataset, followed by 14k steps of fine-tuning on each downstream task (RoboTwin and Vidarc), matching our model’s fine-tuning budget and origin paper settings.
- Pi0.5 [5]: A strong VLA baseline. Due to architectural and optimization differences, Pi0.5 requires more steps to converge on the relatively scarce data for each task and on extensive tasks. To ensure a fair comparison under the multi-task setting, we fine-tune it over the whole dataset instead.

Our model is built upon the Vidar model that was fine-tuned on the downstream task as a weight warm-up initial, augmented with a teacher-forcing mechanism during training, as detailed in Section 2.1. We fine-tune the model with 4k steps separately on each of the two downstream datasets to adjust the model to capture the ability of causal generation. More training details are listed in Appendix B. All models are evaluated on both the RoboTwin benchmark and our real-world deployment.

4.2 Main Experiments

4.2.1 Simulation

Average success rates across 14 tasks and success rates for selected tasks are shown in Table 1, where Vidarc achieves high success rates (**C1**). Vidarc is capable of performing complex tasks with remarkable precision, such as grasping a roller using both arms and opening the articulated laptop. Especially for tasks requiring precise bimanual collaborations, such as handing over the microphone, Vidar achieves higher success rates than Vidar, demonstrating the benefits of closed-loop control. Detailed success rates are provided in Table 6, Appendix C.

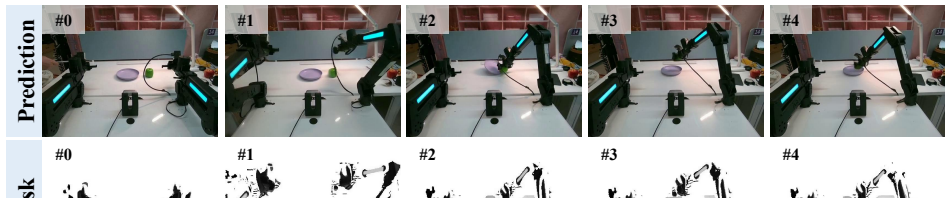
4.2.2 Real-world

Real-world experimental results are summarized in Table 2, where Vidarc achieves superior performance over Vidar and Pi0.5 (**C1**). Across three scenarios, Vidarc achieves good generation ability (**C2**) as well as adaptation to environmental changes (the dynamic case) with error correction abilities (**C3**). Visualizations of error correction cases are shown in Figure 4, demonstrating the advan-

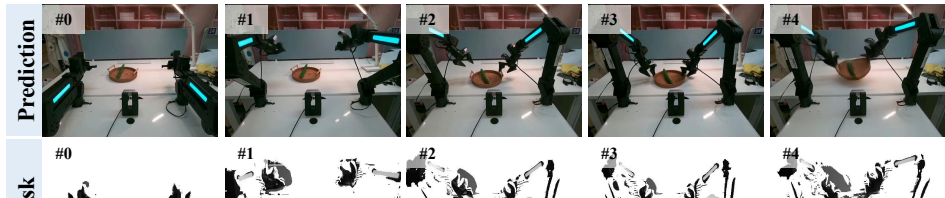
Table 1: Success rates of different methods and configurations over 14 tasks on the RoboTwin benchmark, tested over 20 episodes. “Average*” means the average of all 14 tasks.

Method	Average*	Handover Mic	Open Laptop	Place Can Basket	Place Cans Plasticbox
Pi0.5	52.9%	20.0%	30.0%	35.0%	15.0%
Vidar	71.1%	0.0%	50.0%	50.0%	0.0%
Vidarc	80.7%	65.0%	55.0%	45.0%	85.0%
w/o Embodiment-aware	74.6%	50.0%	65.0%	20.0%	70.0%
w/o Closed-loop	66.8%	25.0%	40.0%	35.0%	50.0%

tages of our closed-loop control and acceleration methods. Detailed success rates are provided in Table 7, Appendix C.



Place The Apple On The Plate: The robot is instructed to pick up the apple and place it on the plate. **During movement, the position of the plate was changed (#0 → #1).** The robot needs to: (1) pick up the green apple, (2) try to place the apple, (3) identify the moved plate, (4) retry and place the apple as required.



Lift The Basket: The robot is instructed to lift the basket with both arms. **During movement, the position of the basket was changed (#0 → #1).** The robot needs to: (1) align the grippers with the basket, (2) try to grasp the basket, (3) realign the grippers with the moved basket, (4) retry and lift the basket as required.

Figure 4: Video predictions, corresponding masks, and executions of Vidarc for dynamic tasks, where its error correction ability is observed.

4.2.3 Speed Evaluation

We also conduct a study on the inference speed of various approaches. All experiments are performed under a unified task duration of 6.4 seconds of real-world execution time. We generate 64 frames for video models, as the video fps is 10. For Pi0.5, we generate 16 actions per chunk, 192

Table 2: Success rates of different methods over real-world scenarios. “Dynamic” means we manually change the position of the targeted object during execution. Vidarc achieves consistently high success rates across all these scenarios.

Method	Average	Seen	Unseen	Dynamic
Pi0.5	41.0%	48.0%	28.0%	48.0%
Vidar	39.0%	72.0%	44.0%	0.0%
Vidarc (Ours)	56.0%	72.0%	56.0%	40.0%

actions in total, as the control frequency of Pi0.5 is 30 Hz. All experiments run on a single NVIDIA A100 GPU.

We evaluate performance mainly using two metrics: latency (measured by time to next chunk execution) and end-to-end generation cost (total chunk generation time). As is shown in Table 3, Vidar suffers from high latency due to its large chunk size and the quadratic complexity of its attention operations; consequently, its latency equals its end-to-end cost, which is substantially high. In contrast, Vidarc reduces latency by 91%, mainly benefiting from its causal generation mechanism. With ongoing hardware advances and further model optimizations—such as quantization and distillation—real-time video generation appears increasingly feasible.

Table 3: Inference speed of different methods (in seconds). Vidarc achieves a lower end-to-end cost and a significantly lower latency than Vidar, making great achievements towards the traditionally fast VLA method Pi0.5.

Method	Latency	Prefill Cost	VAE Cost	Diffusion Cost	End-to-end Cost
Pi0.5	0.482	-	-	-	5.76
Vidar	34.3	-	6.25	26.9	34.3
Vidarc	3.03	0.896	6.45	10.3	24.2

4.3 Ablation Study

We conduct ablation studies on the RoboTwin benchmark to systematically evaluate the contributions of (1) the embodiment-aware diffusion loss and (2) closed-loop control enabled by real-world prefilling. As is shown in Table 1, removing embodiment-aware diffusion loss or closed-loop control lowers success rates, which provides solid evidence for **C4**. Detailed results are in Appendix C, where we also conduct a sensitivity analysis of the hyperparameter η .

4.4 Case Study

As illustrated in Figure 5 and Figure 6, a case study is presented to demonstrate how the re-prefilling mechanism effectively bridges the gap between prediction and execution, thereby enhancing model performance. The upper image sequence was execution environment, the under image was the generated frames of the model.

5 Related Work

Vision-Language-Action Methods for Robotics. Vision-Language-Action (VLA) models leverage natural language instructions as task conditions, enabling multi-task manipulation capabilities that go beyond traditional embodied policies such as Diffusion Policy [38], which are typically restricted to single tasks. However, the main limitation of current VLA methods is their dependence on enormous, task-conditioned datasets—often comprising thousands of trajectories. The scarcity of such large-scale, richly annotated data severely curtails the broader application of VLA models. Recent advances, including OpenVLA [4], Pi0 [39], Pi0.5 [5], and RDT-1B [6], have relied on millions of real robot demonstrations spanning diverse embodiments. Despite the considerable scale of these datasets, VLA models still struggle to generalize robustly to unseen tasks or novel environments. Thus, there remains an urgent need for approaches that are both more data-efficient and more generalizable.

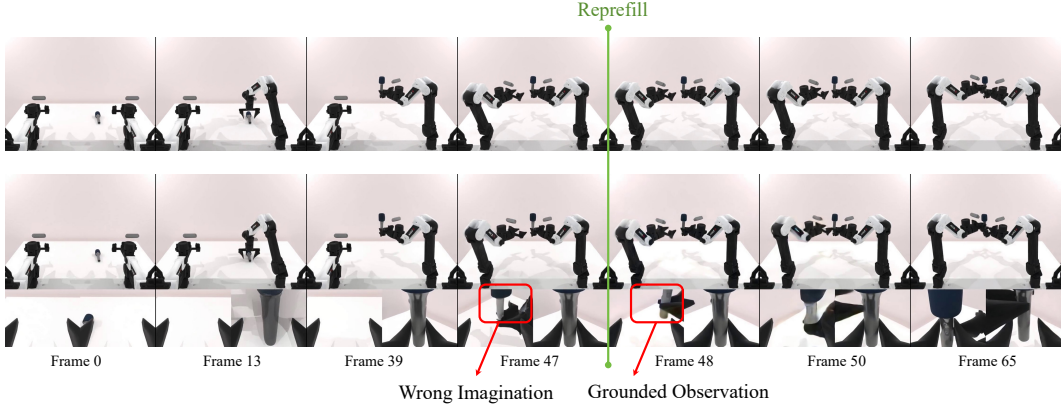


Figure 5: Execution of the method with closed-loop feedback. At frame 47, the model was grounded with real-world sensory data to correct generative drift, ensuring successful task execution.

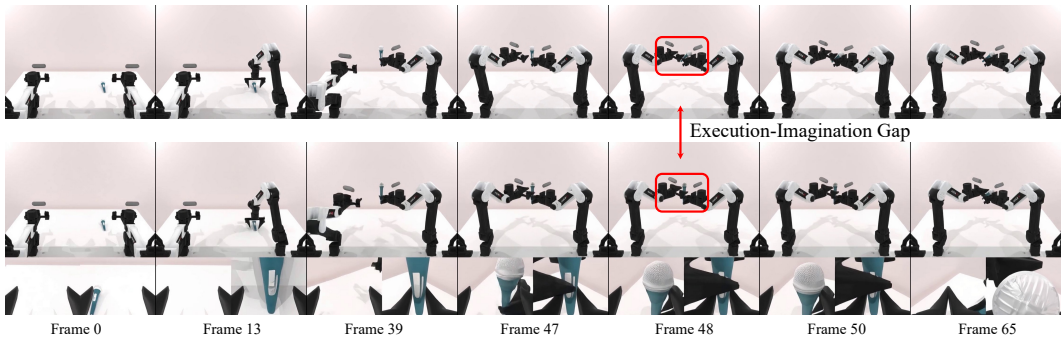


Figure 6: Execution of the method without closed-loop feedback. The model accumulates compounding errors due to ungrounded imagination, leading to eventual task failure.

Video World Models for Robotics. Numerous studies have explored using video world models to decouple image and action spaces. Early approaches [40, 41, 42] utilized RNN-based models and controller architectures to encode visual information and decode actions, respectively. Building on this, recent methods have further explored video-action decoupling, primarily leveraging text-conditioned video generation [17, 43, 44], with extensions including long-horizon planning [45], 3D data utilization [46], diverse datasets [47], and joint video-action latent spaces [48]. Despite all these advances, these methods still suffer from physical inaccuracies, kinematic collapses, and susceptibility to background distractions, especially when confronted with out-of-domain observations. To mitigate these limitations, subsequent work such as Vidar [8] extends this paradigm by introducing a two-stage framework for video generation model training and a masked IDM that ignores visual distractors to focus on the robot’s arms, thereby enhancing generalization to both novel tasks and backgrounds. However, it still exhibits limited video-level controllability and significant computational overhead. In parallel, efficient approaches such as Vidman [49] and VPP [27] have emerged, prioritizing efficiency over the video-action decoupling principle. However, this design choice limits their capability, as they do not model tasks entirely within the visual observation space. This underscores the need for a video world model that simultaneously ensures physical accuracy, optimizes computational cost, and operates within the visual observation space.

Autoregressive Video Diffusion Models. State-of-the-art video generation methods, especially those based on diffusion models, have achieved remarkable progress in the quality and temporal consistency of synthesized content [50, 10, 51]. Inspired by the success of autoregressive frameworks in language modeling, recent studies have increasingly applied autoregressive strategies to video synthesis. Here, pre-trained text-to-video diffusion models generate future frames sequentially, conditioning on previously generated content—examples include NOVA [30], NFD [52], Self-

Forcing [53], Diffusion-Forcing [54], FAR [55], MAGI-1 [56], and CausVid [33]. This framework also supports interactive video generation, as demonstrated by Matrix-Game 2.0 [57]. However, a primary challenge remains: the substantial inference latency introduced by the iterative diffusion denoising process. To address this, key-value (KV) caching is widely adopted to accelerate decoding during inference [30, 57, 53, 33, 56, 52]. Since the timesteps of previous frames are fixed, features from denoised chunks can be cached and efficiently reused for subsequent frames, eliminating redundant computations and significantly enhancing inference efficiency.

6 Conclusion

In this work, we presented Vidarc, a novel framework that integrates an autoregressive embodied video diffusion model with a masked inverse dynamics model to address the challenges of fast, precise control and generalization in data-limited embodied agent settings. By leveraging environmental feedback for closed-loop control, adopting KV cache acceleration, and introducing an embodiment-aware diffusion loss that highlights action-relevant regions, Vidarc overcomes key limitations of existing video-based methods.

Extensive experiments demonstrate that Vidarc achieves significantly higher task success rates, lower latency, and superior generalization to unseen platforms and environments, while also providing robust error correction in real time. Our results highlight the potential of video-based closed-loop methods for scalable and adaptable embodied intelligence, and we believe Vidarc establishes a new direction for efficient and transferable robot learning in complex, dynamic environments.

7 Ethics Statement

Vidarc offers the potential to develop generalist, low-latency robot policies with built-in error correction capabilities for real-world environments. However, deploying such systems in sensitive or home settings may also introduce important safety and privacy concerns.

8 Reproducibility Statement

We include our code in the supplemental materials, covering both the video diffusion model and the masked inverse dynamics model. To support reproducibility, we also plan to open-source our code and model checkpoints. Appendix A provides a detailed description of our dataset, noting that all pre-training datasets are publicly available. Additional information on training and inference procedures is presented in Appendix B.

References

- [1] Oliver Kroemer, Scott Niekum, and George Konidaris. “A Review of Robot Learning for Manipulation: Challenges, Representations, and Algorithms”. In: *J. Mach. Learn. Res.* 22 (2021), 30:1–30:82.
- [2] Jiange Yang et al. “Transferring Foundation Models for Generalizable Robotic Manipulation”. In: *IEEE/CVF Winter Conference on Applications of Computer Vision, WACV 2025, Tucson, AZ, USA, February 26 - March 6, 2025*. IEEE, 2025, pp. 1999–2010.
- [3] Chelsea Finn, Pieter Abbeel, and Sergey Levine. “Model-Agnostic Meta-Learning for Fast Adaptation of Deep Networks”. In: *Proceedings of the 34th International Conference on Machine Learning, ICML 2017, Sydney, NSW, Australia, 6-11 August 2017*. Ed. by Doina Precup and Yee Whye Teh. Vol. 70. Proceedings of Machine Learning Research. PMLR, 2017, pp. 1126–1135.
- [4] Moo Jin Kim et al. “OpenVLA: An Open-Source Vision-Language-Action Model”. In: *Conference on Robot Learning, 6-9 November 2024, Munich, Germany*. Ed. by Pulkit Agrawal, Oliver Kroemer, and Wolfram Burgard. Vol. 270. Proceedings of Machine Learning Research. PMLR, 2024, pp. 2679–2713.
- [5] Physical Intelligence et al. “ $\pi_{0.5}$: a Vision-Language-Action Model with Open-World Generalization”. In: *CoRR* abs/2504.16054 (2025).
- [6] Songming Liu et al. “RDT-1B: a Diffusion Foundation Model for Bimanual Manipulation”. In: *CoRR* abs/2410.07864 (2024).
- [7] Zijian Song et al. “Physical Autoregressive Model for Robotic Manipulation without Action Pretraining”. In: *CoRR* abs/2508.09822 (2025).
- [8] Yao Feng et al. “Vidar: Embodied Video Diffusion Model for Generalist Bimanual Manipulation”. In: *CoRR* abs/2507.12898 (2025).
- [9] Yue Liao et al. “Genie Envisioner: A Unified World Foundation Platform for Robotic Manipulation”. In: *CoRR* abs/2508.05635 (2025).
- [10] Ang Wang et al. “Wan: Open and Advanced Large-Scale Video Generative Models”. In: *CoRR* abs/2503.20314 (2025).
- [11] Yixin Liu et al. “Sora: A Review on Background, Technology, Limitations, and Opportunities of Large Vision Models”. In: *CoRR* abs/2402.17177 (2024).
- [12] Weijie Kong et al. “HunyuanVideo: A Systematic Framework For Large Video Generative Models”. In: *CoRR* abs/2412.03603 (2024).
- [13] Seonghyeon Ye et al. *Latent Action Pretraining from Videos*. 2025.
- [14] Han Xue et al. *Reactive Diffusion Policy: Slow-Fast Visual-Tactile Policy Learning for Contact-Rich Manipulation*. 2025.
- [15] Chuyue Sun et al. *Clover: Closed-Loop Verifiable Code Generation*. 2024.
- [16] Kevin Black, Manuel Y. Galliker, and Sergey Levine. *Real-Time Execution of Action Chunking Flow Policies*. 2025.
- [17] Yilun Du et al. “Learning Universal Policies via Text-Guided Video Generation”. In: *Advances in Neural Information Processing Systems 36: Annual Conference on Neural Information Processing Systems 2023, NeurIPS 2023, New Orleans, LA, USA, December 10 - 16, 2023*. Ed. by Alice Oh et al. 2023.
- [18] Tony Zhao et al. “What makes representation learning from videos hard for control”. In: *RSS 2022 Workshop on Scaling Robot Learning*. 2022.
- [19] Jinheng Xie, Zhenheng Yang, and Mike Zheng Shou. “Show-o2: Improved Native Unified Multimodal Models”. In: *CoRR* abs/2506.15564 (2025).
- [20] Yaron Lipman et al. “Flow Matching for Generative Modeling”. In: *The Eleventh International Conference on Learning Representations, ICLR 2023, Kigali, Rwanda, May 1-5, 2023*. OpenReview.net, 2023.
- [21] Xingchao Liu, Chengyue Gong, and Qiang Liu. “Flow Straight and Fast: Learning to Generate and Transfer Data with Rectified Flow”. In: *The Eleventh International Conference on Learning Representations, ICLR 2023, Kigali, Rwanda, May 1-5, 2023*. OpenReview.net, 2023.

[22] Cheng Lu et al. “DPM-Solver: A Fast ODE Solver for Diffusion Probabilistic Model Sampling in Around 10 Steps”. In: *Advances in Neural Information Processing Systems 35: Annual Conference on Neural Information Processing Systems 2022, NeurIPS 2022, New Orleans, LA, USA, November 28 - December 9, 2022*. Ed. by Sanmi Koyejo et al. 2022.

[23] Jiaming Song, Chenlin Meng, and Stefano Ermon. “Denoising Diffusion Implicit Models”. In: *9th International Conference on Learning Representations, ICLR 2021, Virtual Event, Austria, May 3-7, 2021*. OpenReview.net, 2021.

[24] Philip J. Ball et al. “Genie 3: A New Frontier for World Models”. In: (2025).

[25] Xianglong He et al. *Matrix-Game 2.0: An Open-Source, Real-Time, and Streaming Interactive World Model*. 2025.

[26] Thaddäus Wiedemer et al. *Video models are zero-shot learners and reasoners*. 2025.

[27] Yucheng Hu et al. “Video Prediction Policy: A Generalist Robot Policy with Predictive Visual Representations”. In: *CoRR* abs/2412.14803 (2024).

[28] Hengkai Tan et al. “AnyPos: Automated Task-Agnostic Actions for Bimanual Manipulation”. In: *CoRR* abs/2507.12768 (2025).

[29] Fu-Yun Wang et al. “AnimateLCM: Accelerating the Animation of Personalized Diffusion Models and Adapters with Decoupled Consistency Learning”. In: *CoRR* abs/2402.00769 (2024).

[30] Haoge Deng et al. “Autoregressive Video Generation without Vector Quantization”. In: *The Thirteenth International Conference on Learning Representations, ICLR 2025, Singapore, April 24-28, 2025*. OpenReview.net, 2025.

[31] Jianxiong Gao et al. “LongVie: Multimodal-Guided Controllable Ultra-Long Video Generation”. In: *CoRR* abs/2508.03694 (2025).

[32] Yuanhui Huang et al. “Owl-1: Omni World Model for Consistent Long Video Generation”. In: *CoRR* abs/2412.09600 (2024).

[33] Tianwei Yin et al. “From Slow Bidirectional to Fast Autoregressive Video Diffusion Models”. In: *IEEE/CVF Conference on Computer Vision and Pattern Recognition, CVPR 2025, Nashville, TN, USA, June 11-15, 2025*. Computer Vision Foundation / IEEE, 2025, pp. 22963–22974.

[34] Zipeng Fu, Tony Z. Zhao, and Chelsea Finn. “Mobile ALOHA: Learning Bimanual Mobile Manipulation with Low-Cost Whole-Body Teleoperation”. In: *CoRR* abs/2401.02117 (2024).

[35] Ryan Hoque et al. “EgoDex: Learning Dexterous Manipulation from Large-Scale Egocentric Video”. In: *CoRR* abs/2505.11709 (2025).

[36] AgiBot-World-Contributors et al. “AgiBot World Colosseo: A Large-scale Manipulation Platform for Scalable and Intelligent Embodied Systems”. In: *CoRR* abs/2503.06669 (2025).

[37] Kun Wu et al. “RoboMIND: Benchmark on Multi-embodiment Intelligence Normative Data for Robot Manipulation”. In: *CoRR* abs/2412.13877 (2024).

[38] Cheng Chi et al. “Diffusion Policy: Visuomotor Policy Learning via Action Diffusion”. In: *Robotics: Science and Systems XIX, Daegu, Republic of Korea, July 10-14, 2023*. Ed. by Kostas E. Bekris et al. 2023.

[39] Kevin Black et al. “ π_0 : A Vision-Language-Action Flow Model for General Robot Control”. In: *CoRR* abs/2410.24164 (2024).

[40] David Ha and Jürgen Schmidhuber. “Recurrent world models facilitate policy evolution”. In: *Advances in neural information processing systems* 31 (2018).

[41] Jürgen Schmidhuber. “On Learning to Think: Algorithmic Information Theory for Novel Combinations of Reinforcement Learning Controllers and Recurrent Neural World Models”. In: *CoRR* abs/1511.09249 (2015).

[42] J. Schmidhuber. “An on-line algorithm for dynamic reinforcement learning and planning in reactive environments”. In: *1990 IJCNN International Joint Conference on Neural Networks*. 1990, 253–258 vol.2.

[43] Siyuan Zhou et al. “RoboDreamer: Learning Compositional World Models for Robot Imagination”. In: *Forty-first International Conference on Machine Learning, ICML 2024, Vienna, Austria, July 21-27, 2024*. OpenReview.net, 2024.

[44] Homanga Bharadhwaj et al. “Gen2Act: Human Video Generation in Novel Scenarios enables Generalizable Robot Manipulation”. In: *CoRR* abs/2409.16283 (2024).

- [45] Yilun Du et al. “Video Language Planning”. In: *The Twelfth International Conference on Learning Representations, ICLR 2024, Vienna, Austria, May 7-11, 2024*. OpenReview.net, 2024.
- [46] Haoyu Zhen et al. “TesserAct: learning 4D embodied world models”. In: *arXiv preprint arXiv:2504.20995* (2025).
- [47] Sherry Yang et al. “Learning Interactive Real-World Simulators”. In: *The Twelfth International Conference on Learning Representations, ICLR 2024, Vienna, Austria, May 7-11, 2024*. OpenReview.net, 2024.
- [48] Shuang Li et al. “Unified video action model”. In: *arXiv preprint arXiv:2503.00200* (2025).
- [49] Youpeng Wen et al. “VidMan: Exploiting Implicit Dynamics from Video Diffusion Model for Effective Robot Manipulation”. In: *Advances in Neural Information Processing Systems 38: Annual Conference on Neural Information Processing Systems 2024, NeurIPS 2024, Vancouver, BC, Canada, December 10 - 15, 2024*. Ed. by Amir Globersons et al. 2024.
- [50] Fan Bao et al. “Vidu: a Highly Consistent, Dynamic and Skilled Text-to-Video Generator with Diffusion Models”. In: *CoRR* abs/2405.04233 (2024).
- [51] Yu Gao et al. “Seedance 1.0: Exploring the Boundaries of Video Generation Models”. In: *CoRR* abs/2506.09113 (2025).
- [52] Xinle Cheng et al. “Playing with Transformer at 30+ FPS via Next-Frame Diffusion”. In: *CoRR* abs/2506.01380 (2025).
- [53] Xun Huang et al. “Self Forcing: Bridging the Train-Test Gap in Autoregressive Video Diffusion”. In: *CoRR* abs/2506.08009 (2025).
- [54] Boyuan Chen et al. “Diffusion Forcing: Next-token Prediction Meets Full-Sequence Diffusion”. In: *Advances in Neural Information Processing Systems 38: Annual Conference on Neural Information Processing Systems 2024, NeurIPS 2024, Vancouver, BC, Canada, December 10 - 15, 2024*. Ed. by Amir Globersons et al. 2024.
- [55] Yuchao Gu, Weijia Mao, and Mike Zheng Shou. “Long-Context Autoregressive Video Modeling with Next-Frame Prediction”. In: *CoRR* abs/2503.19325 (2025).
- [56] Hansi Teng et al. “MAGI-1: Autoregressive Video Generation at Scale”. In: *CoRR* abs/2505.13211 (2025).
- [57] Xianglong He et al. “Matrix-Game 2.0: An Open-Source, Real-Time, and Streaming Interactive World Model”. In: *CoRR* abs/2508.13009 (2025).

Table 4: Detailed information about pre-training and fine-tuning datasets.

Dataset	Size	Type	Camera
Egodex	230,949	Human	a movable front camera
Agibot	728,209	Genie-1 Robot	a fixed high camera, a movable left arm camera, and a movable right arm camera
RDT	6,083	Aloha Robot	a fixed front camera, a movable left arm camera, and a movable right arm camera
RoboMind Franka	9,589	Franka Robot	a fixed camera on the opposite side, a fixed left camera, and a fixed right camera
RoboMind Aloha	7,272	Aloha Robot	a fixed front camera, a movable left arm camera, and a movable right arm camera
RoboTwin	1,000	Aloha Robot	a fixed rear camera, a movable left arm camera, and a movable right arm camera
Vidarc	2,307	Aloha Robot	a fixed rear camera, a movable left arm camera, and a movable right arm camera

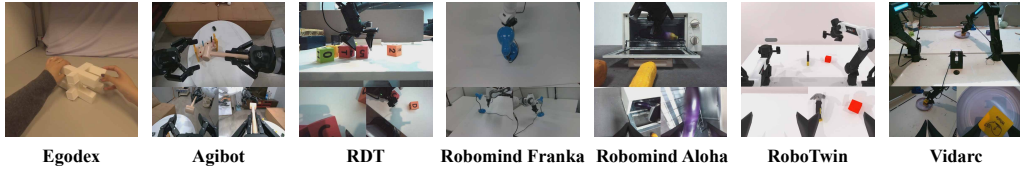


Figure 7: Visualizations of datasets.

A Dataset Details

Detailed dataset information is shown in Table 4. For pre-training, we include human manipulation videos as well as bimanual manipulation videos from 3 different embodiments and various camera configurations. Notably, all these datasets are publicly available. For fine-tuning, we collect 1,000 episodes across 50 tasks on the RoboTwin benchmark; we also collect 2,307 episodes across 219 tasks on our target real-world platform. Notably, the camera and robotic arms for the fine-tuning datasets are unseen and totally different from pre-training. We also provide visualizations of datasets in Figure 7.

We adopt the unified observation space [8] for the formatting of all the datasets, which forms a consistent resolution of 720×640 .

B Model, Training, and Inference Details

B.1 Training

The complete set of training hyperparameters is provided in Table 5.

For video-based models, input videos are downsampled to 10 frames per second (fps) and resized to a resolution of 736×640 . To support classifier-free guidance, the text conditioning is replaced with an empty string with a probability of 0.1 during training.

Our implementation of Vidar adopts the Wan2.2 backbone. The training proceeds in two stages: (i) 10,000 pretraining steps on our internal pretraining dataset, followed by (ii) 14,000 fine-tuning steps on each downstream task (RoboTwin and Vidarc). This two-stage training consumes approximately 4,500 A100 GPU hours in total.

Vidarc is initialized from the reproduced Vidar model and further fine-tuned for an additional 4,000 steps on each downstream task. Notably, the Inverse Dynamics Model (IDM) is shared between Vidar and Vidarc. The IDM is trained separately for 60,000 steps with a weighting coefficient $\lambda = 3 \times 10^{-3}$.

Table 5: Hyperparameters for the training of our experiments.

Hyperparameter	Vidar/Vidarc	IDM	Pi0.5
Number of Parameters	5 Billion	92 Million	2Billion
Learning Rate	2×10^{-5}	5×10^{-4}	2.5×10^{-5}
Batch size	128	128	32
Warm-up	200 Steps	6k steps	1k steps
Optimizer	AdamW	AdamW	AdamW
AdamW β	(0.9, 0.999)	(0.9, 0.999)	(0.9, 0.95)
AdamW ϵ	10^{-8}	10^{-8}	10^{-8}
AdamW Weight Decay	0.1	10^{-2}	10^{-10}

For Pi0.5, due to architectural and optimization differences that lead to slower convergence, we fine-tune the model for 45,000 steps on the simulation dataset and 55,000 steps on the real-world dataset. To ensure a fair comparison across methods, we do not perform task-specific fine-tuning within individual tasks of the dataset (i.e., all tasks within a dataset share the same fine-tuned checkpoint).

B.2 Inference

For the RoboTwin benchmark, we choose 20 sampling steps for both Vidarc and Vidar; the chunk size of Vidarc is set as 16.

For the real-world test, we chose 5 sampling steps for Vidarc and 15 steps for Vidar. In the dynamic scene, we choose a chunk size of 12 for Vidarc and 16 for all other settings.

In speed tests, Vidarc uses 5 sampling steps and generates 8 frames per chunk, whereas the Vidar variant utilizes 20 sampling steps. With our chunk re-prefill method, Vidarc gains an extra 6% end-to-end speed up compared with fully prefill (from 25.8s to 24.2s).

C Additional Results

The complete versions of our simulation and real-world experiments are shown in Table 6 and Table 7.

Detailed ablations are shown in Table 8 and Table 9. We can see that our modules do contribute to the success rates, while the success rates remain high for a wide range of hyperparameter η .

Table 6: Average success rates of different methods over the RoboTwin 2.0 benchmark. Vidarc achieves higher average success rates across these methods.

Task	Pi0.5	Vidar	Vidarc
Click Alarmclock	70.0%	100.0%	100.0%
Click Bell	70.0%	95.0%	100.0%
Grab Roller	75.0%	100.0%	95.0%
Handover Mic	20.0%	0.0%	65.0%
Lift Pot	35.0%	90.0%	80.0%
Open Laptop	30.0%	50.0%	55.0%
Place A2B Left	10.0%	45.0%	35.0%
Place Burger Fries	75.0%	80.0%	80.0%
Place Can Basket	35.0%	50.0%	45.0%
Place Cans Plasticbox	15.0%	0.0%	85.0%
Press Stapler	60.0%	90.0%	100.0%
Shake Bottle	100.0%	100.0%	100.0%
Shake Bottle Horizontally	80.0%	100.0%	100.0%
Stack Bowls Two	65.0%	95.0%	90.0%
Average	52.9%	71.1%	80.7%

Table 7: Real-world evaluations for different methods under three scenarios. The notations “L”, “R”, and “B” denote the left arm, right arm, and both arms, respectively. Vidarc achieves consistently high average success rates across these scenarios.

Seen	Vidarc	Vidar	Pi0.5
Dump the Waste Paper - R	60.0%	100.0%	40.0%
Dump the Waste Paper - L	80.0%	80.0%	100.0%
Grasp the Radish - L	100.0%	80.0%	60.0%
Wipe Table - L	60.0%	40.0%	20.0%
Lift the Basket - B	60.0%	60.0%	20.0%
Average	72.0%	72.0%	48.0%
Unseen	Vidarc	Vidar	Pi0.5
Place the Eggplant - L	40.0%	80.0%	20.0%
Place the Cube - L	60.0%	40.0%	60.0%
Place the Cube - R	40.0%	0.0%	20.0%
Tap Number One - L	100.0%	100.0%	0.0%
Place Steel Wool - R	40.0%	0.0%	40.0%
Average	56.0%	44.0%	28.0%
Dynamic	Vidarc	Vidar	Pi0.5
Dump the Waste Paper - R	20.0%	0.0%	20.0%
Dump the Waste Paper - L	20.0%	0.0%	40.0%
Place the Yellow Item - L	60.0%	0.0%	80.0%
Lift the Basket - B	60.0%	0.0%	0.0%
Place the Apple - R	40.0%	0.0%	100.0%
Average	40.0%	0.0%	48.0%
All Average	56.0%	39.0%	41.0%

Table 8: Average success rates of different configurations over the RoboTwin 2.0 benchmark. “w/o Embodiment-aware” means using the vanilla diffusion loss, and “w/o Closed-loop” means inferring 60 frames using one environmental frame each time.

Task	Vidarc	w/o Embodiment-aware	w/o Closed-loop
Click Alarmclock	100.0%	100.0%	100.0%
Click Bell	100.0%	100.0%	100.0%
Grab Roller	95.0%	75.0%	95.0%
Handover Mic	65.0%	50.0%	25.0%
Lift Pot	80.0%	75.0%	55.0%
Open Laptop	55.0%	65.0%	40.0%
Place A2B Left	35.0%	35.0%	35.0%
Place Burger Fries	80.0%	80.0%	55.0%
Place Can Basket	45.0%	20.0%	35.0%
Place Cans Plasticbox	85.0%	70.0%	50.0%
Press Stapler	100.0%	95.0%	100.0%
Shake Bottle	100.0%	100.0%	95.0%
Shake Bottle Horizontally	100.0%	100.0%	95.0%
Stack Bowls Two	90.0%	80.0%	55.0%
Average	80.7%	74.6%	66.8%

Table 9: Average success rates of different configurations over the RoboTwin 2.0 benchmark. η is the weight hyperparameter in the embodiment-aware loss, and $\eta = 0$ case degrades to the vanilla diffusion loss.

Task	Vidarc ($\eta = 0$)	Vidarc ($\eta = 3$)	Vidarc ($\eta = 10$)
Click Alarmclock	100.0%	100.0%	100.0%
Click Bell	100.0%	100.0%	100.0%
Grab Roller	75.0%	95.0%	85.0%
Handover Mic	50.0%	65.0%	50.0%
Lift Pot	75.0%	80.0%	65.0%
Open Laptop	65.0%	55.0%	65.0%
Place A2B Left	35.0%	35.0%	30.0%
Place Burger Fries	80.0%	80.0%	85.0%
Place Can Basket	20.0%	45.0%	35.0%
Place Cans Plasticbox	70.0%	85.0%	85.0%
Press Stapler	95.0%	100.0%	95.0%
Shake Bottle	100.0%	100.0%	100.0%
Shake Bottle Horizontally	100.0%	100.0%	100.0%
Stack Bowls Two	80.0%	90.0%	85.0%
Average	74.6%	80.7%	77.1%



Figure 8: Our robotic platform.

Table 10: Hardware Information.

Parameters	Values
Cameras	3 RGB Cameras
Degree of Freedom	14
Arm weight	3.9 kg
Arm Valid Payload	1.0 kg
Arm Reach	0.6 m
Arm Repeatability	1 mm
Gripper Range	0 - 80 mm
Gripper Max Force	10 N

D Hardware Details

Hardware details of our robot are shown in Figure 8 and Table 10.

E Usage of Large Language Models

We use large language models to aid and polish writing. We draft the content ourselves and then use large language models to refine it, making the writing clearer, more structured, and easier to understand.